2/p

N62-17745

NASA TN D-1487

TECHNICAL NOTE

D-1487

EFFECTS OF LEADING-EDGE BLUNTNESS ON FLUTTER CHARACTERISTICS OF SOME SQUARE-PLANFORM DOUBLE-WEDGE AIRFOILS AT A MACH NUMBER OF 15.4

By Robert C. Goetz

Langley Research Center
Langley Station, Hampton, Va.

NATIONAL AERONAUTICS AND SPACE ADMINISTRATION

WASHINGTON October 1962

NATIONAL AERONAUTICS AND SPACE ADMINISTRATION

TECHNICAL NOTE D-1487

EFFECTS OF LEADING-EDGE BLUNTNESS ON FLUTTER CHARACTERISTICS OF SOME SQUARE-PLANFORM DOUBLE-WEDGE AIRFOILS AT A MACH NUMBER OF 15.4

By Robert C. Goetz

SUMMARY

Results are presented from a wind-tunnel investigation in helium flow at a :h number of 15.4. The models were square-planform, double-wedge, shaft-mounted ·foils with leading- and trailing-edge radii of 0, 1, 3, and 6 percent chord. general, the tests indicate that bluntness effects on the model flutter char- ;eristics are stabilizing as the leading-edge radius is increased from 0 to)ercent of the chord, but then become destabilizing with further increase in intness.

Results of flutter calculations made by using Newtonian theory aerodynamics l a combination of Newtonian theory and piston theory aerodynamics in conjunc-)n with an uncoupled two-mode analysis are compared with experimental results. : piston-theory results accurately predicted flutter speeds for the models with ;harp leading edge. The Newtonian theory, although conservative, gave better :dictions than the Newtonian-piston theory for the blunt-leading-edge models.

INTRODUCTION

Airfoils on very high-performance aircraft and missiles frequently have inted leading edges to alleviate the aerodynamic-heating problem. It is perti- it, therefore, to investigate the effect of bluntness on the flutter of airfoils the hypersonic range. Double-wedge models have often been used in high-speed itter investigations (refs. 1 to 4) and the effect of leading-edge bluntness on : flutter of such models has been studied in the Mach number region from 0.7 to 36 (ref. 1). It is the purpose of this paper to extend the study of reference 1 a Mach number of 15.4 upon the basis of tests of double-wedge models in helium, which the bluntness of the leading edges was varied systematically over a range radii from 0 to 6 percent of the chord.

In addition to further experimental studies, the need exists for evaluation available analytical methods for the prediction of aeroelastic phenomena at gh speeds. In this report two-degree-of-freedom flutter calculations were made r the various models tested by using the first two uncoupled modes in conjunc- on with Newtonian theory aerodynamics and a combination of Newtonian and piston theory aerodynamics. These two theoretical methods were evaluated by compariso with the experimental results.

SYMBOLS

b wing semispan, ft

f_f flutter frequency, cps

f_h flapping frequency, cps

f_n natural frequency of nth mode (n = 1 and 2), cps

f_α pitching frequency (bending degree of freedom restrained), cps

I_α mass moment of inertia about pitch axis, slug-ft^2

m mass, slugs

r_α radius of gyration of model, referred to pitch axis, $\sqrt{\frac{I_\alpha}{mb^2}}$, nondimensi

V free-stream velocity, ft/sec

x_0 pitch-axis location measured from leading edge, percent chord

x_{cg} distance from leading edge to center of gravity, percent chord

y_{cg} distance from root chord to center of gravity, percent semispan

μ nondimensional mass ratio (ratio of mass of model to mass of volume of test medium contained in a solid generated by revolving each chord about its midpoint, length of solid being wing semispan)

ω_f flutter frequency, radians/sec

ω_n frequency of nth mode (n = 1, 2), radians/sec

Subscripts:

av average

div divergence

exp experimental results

th theoretical results

APPARATUS

The tests were performed in the 24-inch-diameter nozzle of the Langley hyper-
ıic aeroelasticity tunnel, which uses helium as a test medium. The tunnel has
:ontoured nozzle designed to generate a uniform flow at a Mach number of about
A photograph of this blowdown tunnel is shown in figure 1.

Helium is supplied to the stagnation chamber at pressures up to 1,200 lb/sq in.,
ɔm which dynamic pressures up to 595 lb/sq ft are obtainable. The downstream
ı of the tunnel is connected to a vacuum chamber which can be operated at pres-
·es as low as 1/2 inch of mercury absolute. With the available high-pressure
ium supply, test runs were of approximately 5-second duration.

Test-section Mach number distributions as obtained from impact-tube surveys
presented in figures 2(a) and 2(b). Figure 2(a) shows that the average Mach
ıber at a given point was about 15.4. Also shown is that the Mach number
ıained practically constant for a given stagnation pressure. Figure 2(b) shows
ıt there was little variation of Mach number over the length of the test section.

The models were mounted on a reflection plane which was supported 6.8 inches
ɔm the tunnel wall as shown in figure 3. The reflection-plane support structure
designed to insure that the model was out of the tunnel boundary layer and in
region of uniform flow. A sketch of the tunnel test section showing its over-
dimensions and the location of the model and its support structure is pre-
ıted in figure 4. Mach number surveys have been made from the reflection plane
ross the diameter of the test section along the model location. The results
shown in figure 5. It appears that the reflection-plane leading edge was in
region of undisturbed flow; however, a disturbed region was building up along
reflection-plane surface as the flow moved rearward. Even so, in the vicinity
the model trailing edge, the disturbed region covered less than 15 percent of
span. The tip of the model was in uniform flow and not in the boundary layer
ɔm the opposite tunnel wall.

Provision was made for a clamping device which was located at the junction
the model shaft and reflection plane in the support structure. This clamping
vice was used to restrain the model during the tunnel starting transient, and
so to avoid destruction of the model when flutter occurred. Thus the same model
uld be used for more than one test.

MODELS

The two series of models tested each had semispan aspect ratios of 1.0, zero
eep, double-wedge profile shapes, and no taper. The difference between the two
ries was that one had a 10-inch semispan whereas the other had a 6-inch semi-
an. Each series consisted of four models of varying leading-edge bluntness;
ey had leading- and trailing-edge radii of 0, 1, 3, and 6 percent of their chord.
photograph of the 10-inch models is shown in figure 6. The models were sup-
rted by a shaft which was an integral part of the aluminum-alloy core of the

model and which was clamped at the tunnel wall. Holes were drilled in the cor and lead strips were added in order to achieve the desired mass and inertia pr erties. Then balsa wood was glued to the core to form the airfoil contour. Th model construction is shown in figure 7. The models were designed as rigid bodies mounted on a soft spring (the shaft) in order to provide a simple model with well-defined structural properties. Therefore, the structural variables were isolated and the aerodynamic effects more pronounced.

PHYSICAL PARAMETERS

The mass parameters of the models are listed in table I along with pertine dimensions. The mass of the model shaft is not included in the data shown. Th pitch axis of all the models was at the 35-percent-chord position with the pane center of gravity located at 53.5(±0.9) percent chord and 50.0(±1.5) percent se span. All models were vibrated with an interrupted-air-jet shaker to determine the natural frequencies and nodal patterns. Typical nodal patterns for the mod are shown in figure 8. In all cases examined, the third and fourth natural fre quencies were well above the first and second natural frequencies. The first t coupled frequencies as well as the first two uncoupled frequencies are listed i table I. The first uncoupled frequency, flapping, was calculated by using the measured mass properties. The second uncoupled frequency, pitching, was found experimentally. Because the second natural node line was skewed, it was necess to restrict the model deflection at an assumed pitch-axis location, 35 percent chord at the model tip, in order to measure the uncoupled pitching frequency. first two uncoupled mode shapes for the models were determined in the following manner: For the flapping mode the model was vibrated at its first natural frequency by means of an air shaker, and the amplitude of vibration was measured a various stations with time-exposure photographs. This mode shape is presented figure 9(a). Because a slight amount of pitching is evident, the model was assumed to be rigid and the deflection along the 50-percent-chord line (center-of-gravity location) was used in the calculations. For the pitching mode the model was vibrated in its restricted uncoupled pitching mode, and time-exposure photographs were used to measure the deflection. The pitching-mode shape is pr sented in figure 9(b) and was used in the flutter calculations. In addition, t fundamental uncoupled mode shape was calculated for a system consisting of a ri beam on a flexible, weightless shaft and the result agreed well with the experimentally determined uncoupled flapping-mode shape.

TEST PROCEDURE

Models were mounted in the test section at zero angle of attack. After installation in the tunnel and just prior to the test run, the measurements for the first two natural frequencies of the model were checked. The tunnel was th evacuated to a low pressure. The model was restrained, and a control valve upstream of the test section was opened and flow established at a low dynamic pre sure. At this time the model was released and, with the Mach number remaining constant, dynamic pressure was increased until flutter was encountered or the ximum tunnel operating conditions were reached. At that point the model was ain restrained and the tunnel flow stopped. Stagnation temperature and pressure re recorded on an oscillograph throughout the test. Signals from resistance-pe strain gages mounted on the model shaft were also recorded and their response s used to determine the occurrence of flutter and the flutter frequency. These ta were later correlated with the tunnel conditions. High-speed motion pictures the flutter of most of the models were obtained.

RESULTS AND DISCUSSION

Experimental Investigation

The basic data from the tests are presented in table II. The test-section nditions at flutter as well as the flutter frequency ratio ω_f/ω_2 and velocity-dex parameter $V/b\omega_2\sqrt{\mu}$ are listed for each test run. The experimental results om table II are presented in figures 10 and 11 as the variation of the velocity-dex parameter and frequency ratio with leading-edge radius. In figure 12, some the data of reference 1 are combined with the present data and presented as the riation of velocity-index parameter $V/b\omega_2\sqrt{\mu}$ with Mach number for the various dels.

Examination of the data for the 10-inch model in figure 10 reveals that the utter speed increases as the leading-edge radius is increased from 0 to 1 per-nt of the chord, and then the trend reverses; that is, the flutter speed creases with further bluntness. During tests of the 10-inch model with a ading-edge radius of 6 percent chord, the tunnel would not start; that is, the low could not be established in the test section at $M = 15.4$.

In an attempt to investigate the 6-percent-chord leading-edge radius, and lso to explore size effects, the 6-inch-chord models were constructed and tested. e flutter trend remained the same for the models with the 0-, 1-, and 3-percent-ord leading-edge radii, as can be seen in figure 10. However, no flutter was countered for the 6-percent-chord leading-edge models; instead the model iverged. The divergence was quite abrupt, the model striking the reflection lane with little or no oscillatory displacement.

The flutter mode was a combination of the flapping and pitching natural odes. Figure 11 shows the flutter frequency ratio as a function of leading-dge radii. For the models with sharp and 1-percent-chord leading edges, the lutter frequency ratios ranged from 0.47 to 0.59, whereas for the models with -percent-chord radii, it decreased to between 0.31 and 0.37. From this result nd from observations of the films of the test it is believed that for the models ith 3-percent-chord radius the flutter condition was approaching the divergence ondition and thus the flutter frequency was forced toward zero.

In figure 12, some of the results of reference 1 have been combined with hose reported in this paper to show the variation of the velocity-index param-ter over a wide range of Mach number. The models with sharp and 1-percent-hord radius exhibit the same trend of consistently increasing values of the parameter with increasing Mach number. The model with 3-percent-chord radius warrants special attention, for in this case the velocity-index parameter, rath than increasing with Mach number, reverses the trend between $M = 7.0$ and 15.4; and at $M = 15.4$ the parameter has the same value as at $M = 2.6$. The models with leading-edge radii of 6 percent of the chord diverged at all Mach numbers above about 1.6. At a Mach number of 15.4, the value of the velocity-index parameter for divergence was about the same as at Mach 1.6. It should be noted that over the Mach number range the minimum value of the velocity-index paramete occurred near $M = 1$.

Theoretical Investigation

Lighthill, in reference 5, developed a simplified aerodynamic theory which has become known as "piston theory." Ashley and Zartarian (ref. 6) have applie it to the flutter problem. They point out that the theory does not consider three-dimensional effects, but it should be noted that with increase in Mach nu ber these effects should become less important. In addition, a requirement for good accuracy is that the downwash velocity at the wing surface divided by the speed of sound must be less than 1. This requirement, besides being a limit on airfoil thickness, also implies that piston theory will not be applicable near the leading edge of blunt-nosed airfoils where the surface slopes are large. It has been suggested in reference 7 that the use of Newtonian theory would remove the limitation due to bluntness. The Newtonian theory would be used over the leading-edge radius and piston theory over the remainder of the airfoil. Newtor theory, even though it is based upon simple impact considerations, has given goc aerodynamic predictions in hypersonic flow (ref. 8).

Two-degree-of-freedom flutter calculations were made for the models by usir the first two uncoupled modes in conjunction with modified Newtonian-piston thec and modified Newtonian theory aerodynamics. The calculated uncoupled flapping frequencies and the experimentally determined pitching frequencies given in table I were used in the solution of the flutter determinant. Generalized mass terms were calculated from the experimentally measured mass, moment of inertia about the pitch axis, and center-of-gravity position as given in table I. The mass of the shaft was not included, and the panel mass was assumed to be uniform over the span, which was very nearly the case. The results of these calculation are listed in table III and presented in figures 13 and 14. Figure 13 presents the ratio of experimental to calculated flutter speed as a function of leading-edge bluntness. In figure 13(a) the calculated flutter-speed data are presented for the 10-inch-chord models. There was excellent agreement between experiment and piston theory for the sharp-leading-edge models, whereas the Newtonian theor was unconservative. With increase in bluntness both the Newtonian-piston and Newtonian theories became conservative, with the Newtonian theory giving slightl better agreement with the experiment. Figure 13(b) presents the same data for t 6-inch-chord models with about the same results; although the agreement for the blunt airfoils is better.

The ratios of experimental to theoretical flutter frequency are presented i figure 14 as a function of leading-edge radius. The Newtonian-piston theory pre dicted the flutter frequency somewhat more accurately, although neither theory

dicted the decrease in flutter frequency which occurred for the 3-percent-
ding-edge model.

In an effort to investigate the divergence of some of the models analytically, e Newtonian theory flutter determinant was expanded and the flutter frequency t equal to zero. These divergence results are presented in figure 15 along with e Newtonian flutter theory and the average experimental results. According to e theory the flutter speed of each model was lower than its divergence speed. t it should be noted that the calculated divergence speed was approaching the utter speed with increase in model bluntness.

SUMMARY OF RESULTS

Wind-tunnel tests at a Mach number M of 15.4 on square-planform, all-movable-ntrol-type models having leading- and trailing-edge radii from 0 to 6 percent ord and double-wedge profiles indicated a definite effect of airfoil bluntness their aeroelastic characteristics. The tests indicated that bluntness effects re stabilizing as the leading-edge radius was increased from 0 to about 1 per-nt of the chord. A further increase in bluntness had a destabilizing effect on e flutter characteristics.

For the models with sharp leading edges and 1-percent-chord leading-edge dii the stabilizing trend was consistent with data obtained at lower Mach num-rs in NASA TN D-984. For the 3-percent-chord leading-edge model there was a versal in trend with Mach number between M = 7.0 and M = 15.4. Within this ch number range there was a destabilizing trend, and at M = 15.4 the model countered flutter at about the same velocity-index parameter as at M = 2.6. is decrease in stability was believed to be due to the fact that the flutter eed was close to the divergence speed. At M = 15.4, increasing the airfoil untness to 6 percent of the chord led to divergence, as it did at lower Mach mbers. However, the velocity-index parameter for divergence at M = 15.4 creased to about the same value as at M = 1.6.

Flutter calculations made by using Newtonian theory aerodynamics and a com-nation of Newtonian theory and piston theory aerodynamics, both in conjunction th an uncoupled two-mode analysis, indicated that the Newtonian-piston theory, though conservative, more closely predicted the flutter speed for the models th blunt leading edges. Neither theory predicted the flutter frequency well.

The Newtonian theory failed to predict divergence for the 6-percent-chord ading-edge model, but instead predicted a flutter speed lower than the diver-nce speed. The theory did show that the divergence speed was approaching the utter speed with increasing leading-edge bluntness.

ngley Research Center,
National Aeronautics and Space Administration,
Langley Station, Hampton, Va., July 17, 1962.

REFERENCES

1. Hanson, Perry W.: Aerodynamic Effects of Some Configuration Variables on th Aeroelastic Characteristics of Lifting Surfaces at Mach Numbers From 0.7 t 6.86. NASA TN D-984, 1961.

2. Morgan, Homer G., and Miller, Robert W.: Flutter Tests of Some Simple Model at a Mach Number of 7.2 in Helium Flow. NASA MEMO 4-8-59L, 1959.

3. Martuccelli, John R.: Flutter Model Tests at Mach Numbers 1.5-5.0. WADC T Rep. 59-407, U.S. Air Force, Sept. 1959.

4. White, Richard P., Jr., King, Stephen R., and Balcerak, John C.: Flutter Mo Tests at Hypersonic Speeds M = 5 to 7. WADD Tech. Rep. 60-328, U.S. Air Force, May 1960.

5. Lighthill, M. J.: Oscillating Airfoils at High Mach Number. Jour. Aero. Sc vol. 20, no. 6, June 1953, pp. 402-406.

6. Ashley, Holt, and Zartarian, Garabed: Piston Theory - A New Aerodynamic Too for the Aeroelastician. Jour. Aero. Sci., vol. 23, no. 12, Dec. 1956, pp. 1109-1118.

7. Morgan, Homer G., Runyan, Harry L., and Huckel, Vera: Theoretical Considera tions of Flutter at High Mach Numbers. Jour. Aero. Sci., vol. 25, no. 6, June 1958, pp. 371-381.

8. Wells, William R., and Armstrong, William O.: Tables of Aerodynamic Coeffi- cients Obtained From Developed Newtonian Expressions for Complete and Part Conic and Spheric Bodies at Combined Angles of Attack and Sideslip With So Comparisons With Hypersonic Experimental Data. NASA TR R-127, 1962.

[x_0 = 35 percent chord]

Model (a)	Mass, m, slugs	x_{cg}, % chord	y_{cg}, % semispan	I_α, slug-ft^2	r_α^2	Wing semichord, b, ft	Wing semispan, ft	Maximum thickness, percent chord	f_1, cps	f_2, cps	f_α, cps	f_1/f_α	f_1/f_2	f_h, cps
0-A-10-1	0.0348	52.6	49.7	2.7342 × 10^{-3}	0.452	0.417	0.833	9.0	6.0	21.3	17.8	0.337	0.282	7.2
0-B-10-1	.0422	53.5	49.8	3.3250	.453				7.4	25.3	21.8	.339	.292	9.3
0-C-10-1	.0486	53.1	49.0	3.7133	.440				9.1	32.3	26.7	.341	.282	10.9
0-A-10-2	.0486	53.1	49.0	3.7133	.440				5.5	19.8	15.7	.350	.278	6.1
0-A-10-3	.0348	52.6	49.7	2.7342	.452				6.4	22.2	18.2	.351	.288	7.2
1-A-10-1	.0364	53.0	50.5	2.8800	.455			11.0	5.9	20.0	17.8	.331	.295	7.1
1-B-10-1	.0465	53.4	50.4	3.6092	.446				7.3	26.8	22.4	.326	.272	8.7
1-C-10-1	.0495	53.2	49.1	3.8650	.449				9.1	31.9	26.3	.346	.285	10.9
1-A-10-2	.0495	53.2	49.1	3.8650	.449				5.4	19.7	16.5	.330	.277	6.1
3-A-10-1	.0429	52.6	50.0	3.3133	.444			14.0	5.7	21.1	17.9	.318	.270	6.5
3-B-10-1	.0502	52.7	51.5	3.8158	.437				6.8	25.2	21.2	.321	.270	8.4
3-C-10-1	.0552	53.5	51.4	4.3133	.450				8.5	31.3	26.1	.326	.272	10.2
3-A-10-2	.0552	53.5	51.4	4.3133	.450				5.2	19.3	16.5	.315	.269	6.2
6-A-10-1	.0496	52.9	51.4	3.9258	.455			20.0	5.2	19.5	16.5	.315	.267	6.2
6-B-10-1	.0540	52.9	51.0	4.4008	.469				6.7	24.0	20.5	.326	.279	8.0
6-C-10-1	.0601	53.6	51.1	4.9475	.473				8.3	29.6	25.0	.332	.280	9.9
0-A-6-1	.0167	53.3	49.2	.445	.426	.250	.500	9.0	6.3	25.5	21.0	.300	.247	6.6
0-A-6-2	.0170	54.1	49.2	.458	.431				6.2	25.2	20.4	.304	.246	6.5
0-A-6-3	.0163	54.3	50.8	.434	.426				6.4	25.8	20.9	.306	.248	6.7
1-A-6-1	.0165	54.3	50.0	.442	.429			11.0	6.3	24.9	20.5	.307	.253	6.6
1-A-6-2	.0170	54.3	49.3	.456	.429				6.5	25.5	21.3	.305	.255	6.6
1-A-6-3	.0168	53.3	50.0	.441	.420				6.3	24.8	20.5	.307	.254	6.6
3-A-6-1	.0175	53.3	50.0	.438	.406			14.0	6.4	26.1	21.4	.300	.245	6.5
3-A-6-2	.0167	53.4	49.5	.430	.412				6.4	26.3	21.4	.300	.243	6.6
3-A-6-3	.0172	54.2	49.5	.443	.412				6.4	26.5	21.3	.300	.242	6.6
6-A-6-1	.0185	53.2	51.5	.464	.401			20.0	6.1	25.9	20.2	.302	.236	6.4
6-A-6-2	.0184	53.2	50.0	.460	.400				6.0	24.8	19.9	.302	.242	6.3
6-A-6-3	.0183	53.2	50.0	.456	.400				5.9	24.2	19.7	.300	.244	6.2
6-A-6-4	.0233	53.2	50.5	.582	.400				5.7	21.2	17.9	.318	.269	6.0

[a]In the model designation the first integer indicates leading-edge radius in percent chord; the letter indicates the stiffness level of the model (where A < B < C); the next number is the chord and semispan in inches; and the last number is the model number in a group of similar models.

TABLE II.- COMPILATION OF TEST RESULTS

Model (a)	Run	Mach number	Dynamic pressure, lb/sq ft	Density, slugs/cu ft	Speed of sound, ft/sec	μ	V, ft/sec	ω_2, radians/sec	$V/b\omega_2\sqrt{\mu}$	ω_f, radians/sec	ω_f/ω_2
0-B-10-1	1	15.50	512	2.817×10^{-5}	389	3,291.7	6,029.5	159.0	1.585	81.7	0.514
0-A-10-3	2	15.30	306	1.889	372	4,046.5	5,691.6	139.5	1.538	82.0	.588
0-A-10-2	3	15.20	287	1.478	410	7,221.4	6,232.0	124.4	1.414	66.9	.538
1-A-10-1	4	15.40	401	1.992	412	4,013.2	6,344.8	125.7	1.911	69.8	.555
1-A-10-1	5	15.40	398	1.987	411	4,026.5	6,329.4	125.7	1.903	----	-----
1-A-10-2	6	15.40	432	2.277	400	4,778.0	6,160.0	123.8	1.726	72.3	.584
3-B-10-1	7	15.40	405	1.856	429	5,940.8	6,606.6	158.3	1.298	54.0	.341
3-B-10-1	8	15.50	474	2.466	400	4,474.2	6,200.0	158.3	1.404	55.9	.353
0-A-6-1	9	15.30	313	1.492	423	11,376.0	6,471.9	160.22	1.515	78.5	.490
1-A-6-2	10	15.45	429	2.213	403	7,823.3	6,226.4	160.22	1.757	75.4	.471
1-A-6-3	11	15.30	340	1.728	410	9,899.8	6,273.0	155.80	1.619	77.3	.496
3-A-6-1	12	15.20	280	1.361	422	13,089.0	6,414.4	163.99	1.368	59.7	.364
3-A-6-2	13	15.20	297	1.444	422	11,777.2	6,414.4	165.25	1.431	52.5	.318
6-A-6-1	14	15.20	[b]292	1.361	431	13,836.9	[b]6,551.2	162.73	[b]1.369	----	-----
6-A-6-1	15	15.00	[b]173	.933	406	20,196.5	[b]6,090.0	162.73	[b]1.053	----	-----
6-A-6-2	16	15.00	[b]180	.961	408	19,491.5	[b]6,120.0	155.82	[b]1.125	----	-----
6-A-6-4	17	15.35	[b]415	2.258	395	10,448.4	[b]6,063.3	133.2	[b]1.068	----	-----

[a]In the model designation the first integer indicates leading-edge radius in percent chord; the letter indicates the stiffness level of the model (where $A < B < C$); the next number is the chord and semispan in inches; and the last number is the model number in a group of similar models.

[b]Divergent condition.

TABLE III.- COMPILATION OF THEORETICAL CALCULATIONS

Model (a)	Run	Flutter calculations, Newtonian theory: V_{th}, ft/sec	Flutter calculations, Newtonian theory: $\omega_{f,th}$, radians/sec	Flutter calculations, Newtonian theory: $\frac{V_{exp}}{V_{th}}$	Flutter calculations, Newtonian theory: $\frac{\omega_{f,exp}}{\omega_{f,th}}$	Flutter calculations, Newtonian-piston theory: V_{th}, ft/sec	Flutter calculations, Newtonian-piston theory: $\omega_{f,th}$, radians/sec	Flutter calculations, Newtonian-piston theory: $\frac{V_{exp}}{V_{th}}$	Flutter calculations, Newtonian-piston theory: $\frac{\omega_{f,exp}}{\omega_{f,th}}$	Divergence calculations, Newtonian theory: Divergent dynamic pressure, lb/sq ft	Divergence calculations, Newtonian theory: $\frac{V}{b\omega_2\sqrt{\mu}}$
0-B-10-1	1	6,662.3	111.9	0.905	0.730	5,997.2	103.0	1.005	0.793	4,648	4.789
0-A-10-3	2	6,493.3	96.7	.877	.848	5,758.5	89.8	.988	.913	2,882	4.737
0-A-10-2	3	7,220.6	80.2	.863	.834	6,385.5	74.3	.976	.900	2,764	4.620
1-A-10-1	4	5,367.2	85.2	1.182	.819	4,952.9	79.4	1.281	.879	1,544	3.582
1-A-10-2	6	5,540.5	78.6	1.112	.920	5,025.0	73.6	1.226	.982	1,809	3.582
3-B-10-1	7	6,492.7	93.1	1.018	.580	6,164.4	90.0	1.072	.600	1,928	2.836
3-B-10-1	8	5,624.0	93.0	1.102	.601	5,345.4	89.9	1.160	.622	1,928	2.836
0-A-6-1	9	7,750.7	106.6	.835	.736	6,781.1	100.4	.954	.782	3,145	4.593
1-A-6-2	10	5,931.5	102.9	1.050	.733	5,390.3	97.2	1.155	.776	1,990	3.499
1-A-6-3	11	6,232.5	96.9	1.006	.798	5,684.0	91.4	1.104	.846	1,739	3.488
3-A-6-1	12	6,342.1	92.1	1.011	.648	5,916.8	89.9	1.084	.664	1,022	2.490
3-A-6-2	13	6,005.1	92.2	1.068	.569	5,607.2	88.8	1.144	.591	975	2.444
6-A-6-1	14	5,306.9	87.5	1.234	-----	5,096.3	86.5	1.285	-----	648	1.936
6-A-6-1	15	6,513.7	87.6	.935	-----	6,006.6	86.6	1.014	-----	648	1.928
6-A-6-2	16	6,223.9	87.0	.983	-----	5,913.0	86.3	1.035	-----	650	2.037
6-A-6-4	17	3,706.6	74.4	1.636	-----	3,537.1	74.3	1.714	-----	533	2.013

[a]In the model designation the first integer indicates leading-edge radius in percent chord; the letter indicates the stiffness level of the model (where $A < B < C$); the next number is the chord and semispan in inches; and the last number is the model number in a group of similar models.

Leading-edge radius, % chord	$\left(\frac{V_{th}}{b\omega_2}\sqrt{\mu}\right)_{av}$ for - Flutter	Divergence
0	1.714	4.685
1	1.654	3.565
3	1.331	2.600
6	.964	1.978

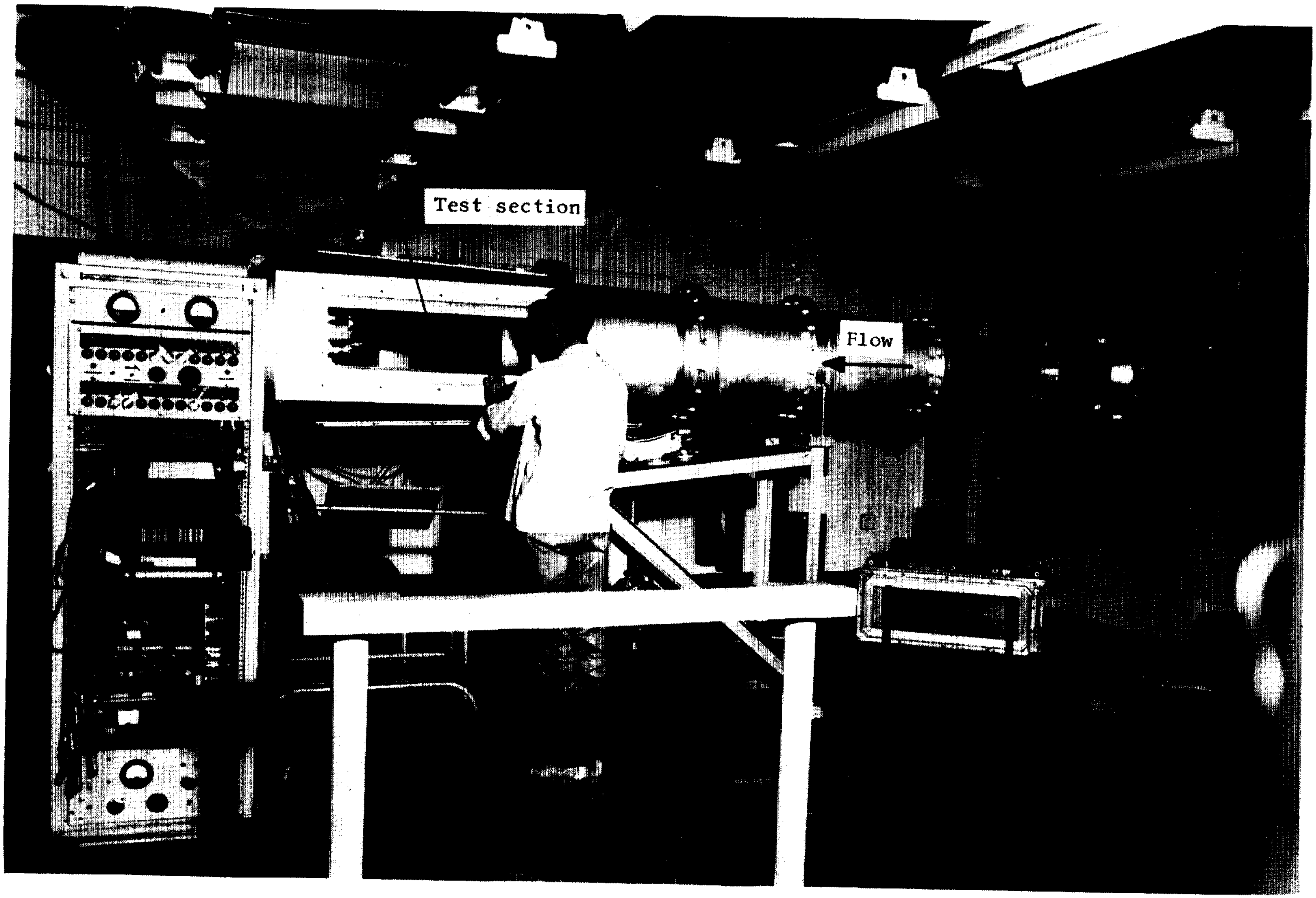

Figure 1.- Langley hypersonic aeroelasticity tunnel. L-61-7414.1

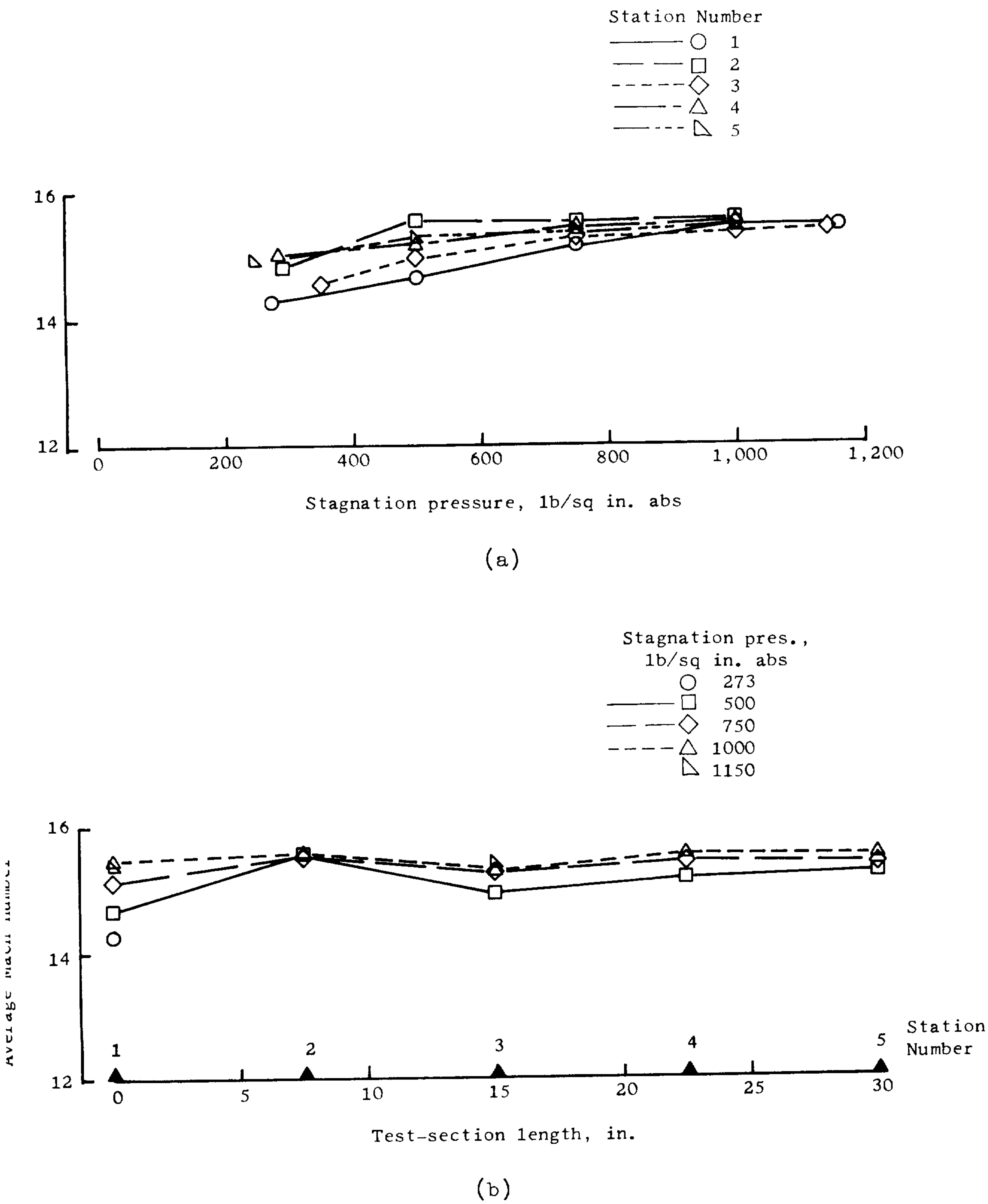

Figure 2.- Mach number survey along tunnel test-section length.

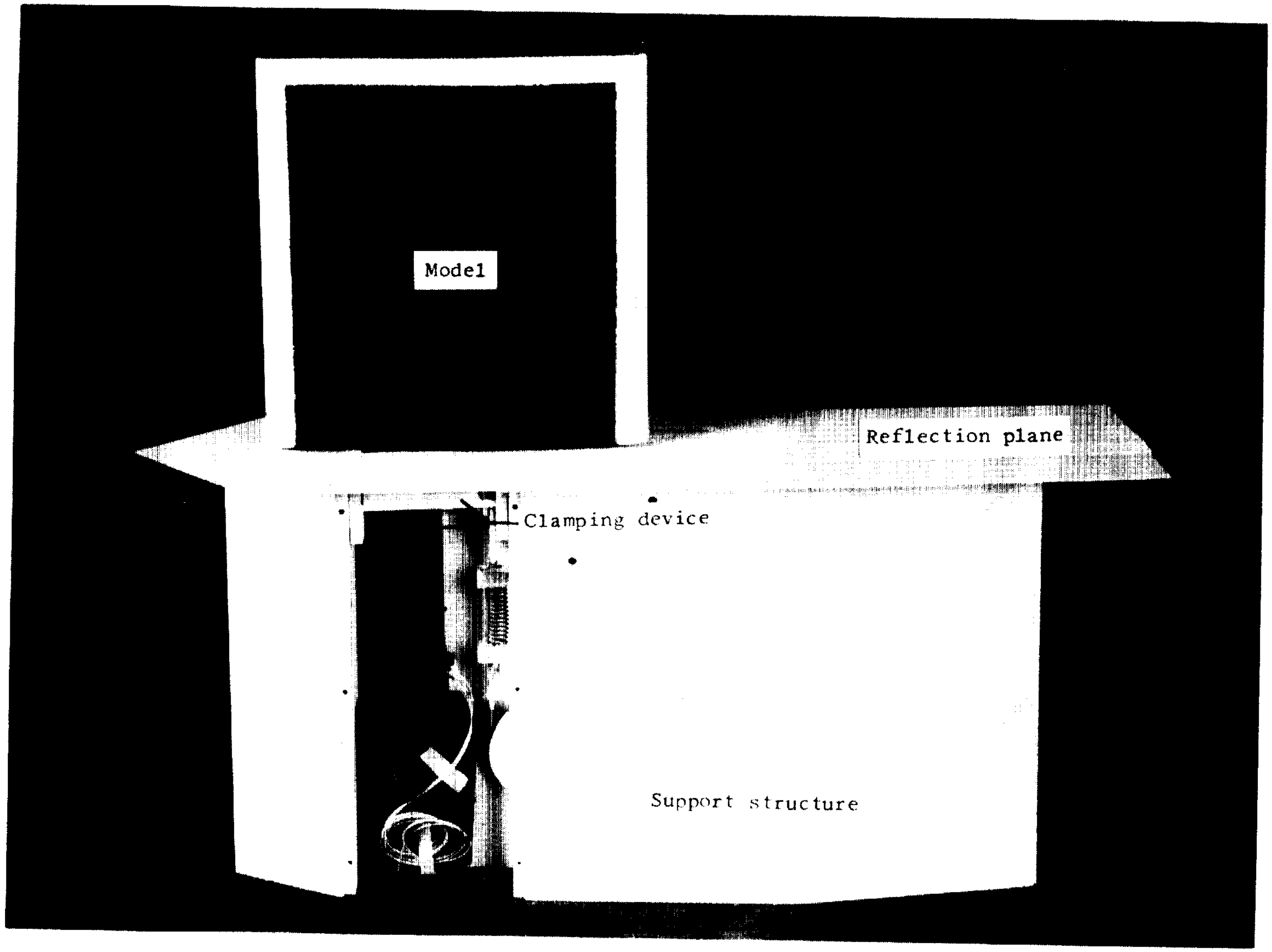

Figure 3.- Model support structure. L-62-3321.1

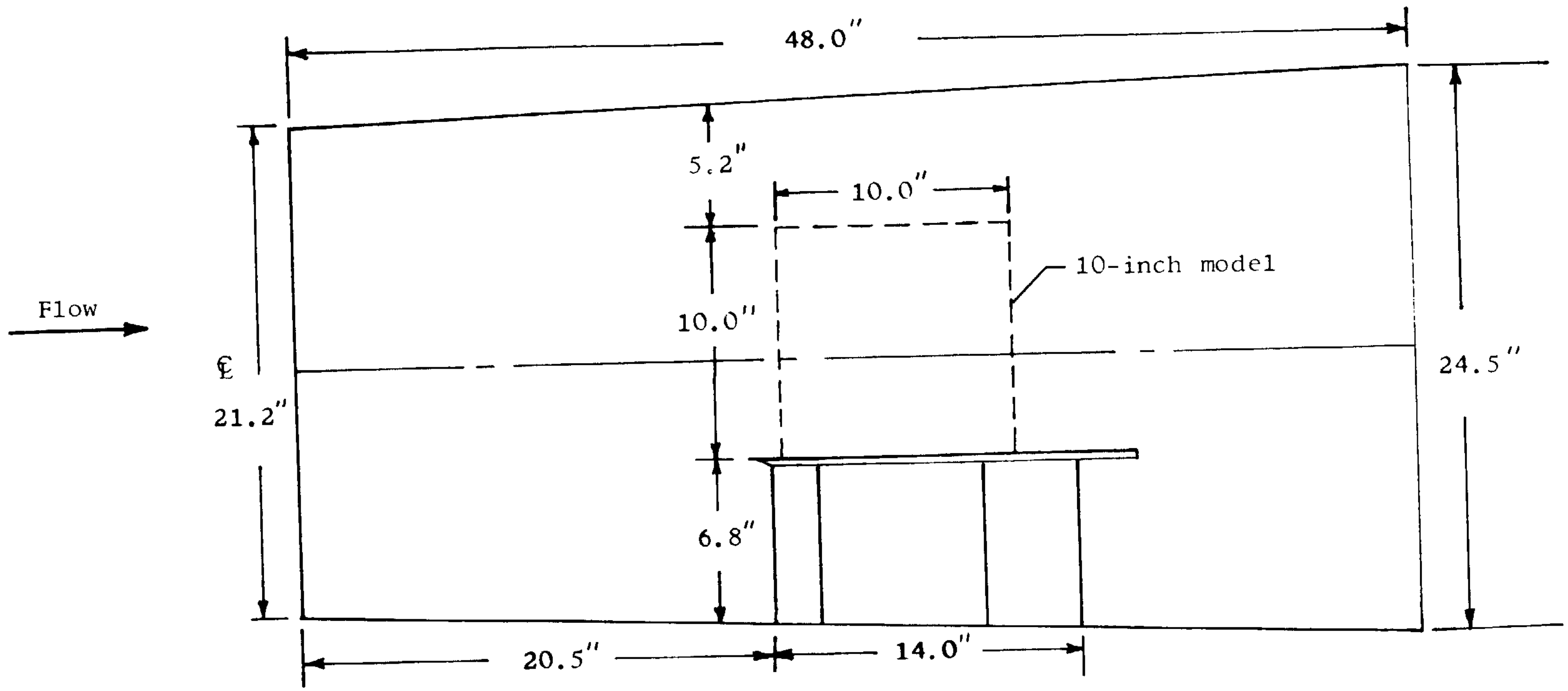

Figure 4.- Location of model support structure in tunnel test section. All dimensions are in inches.

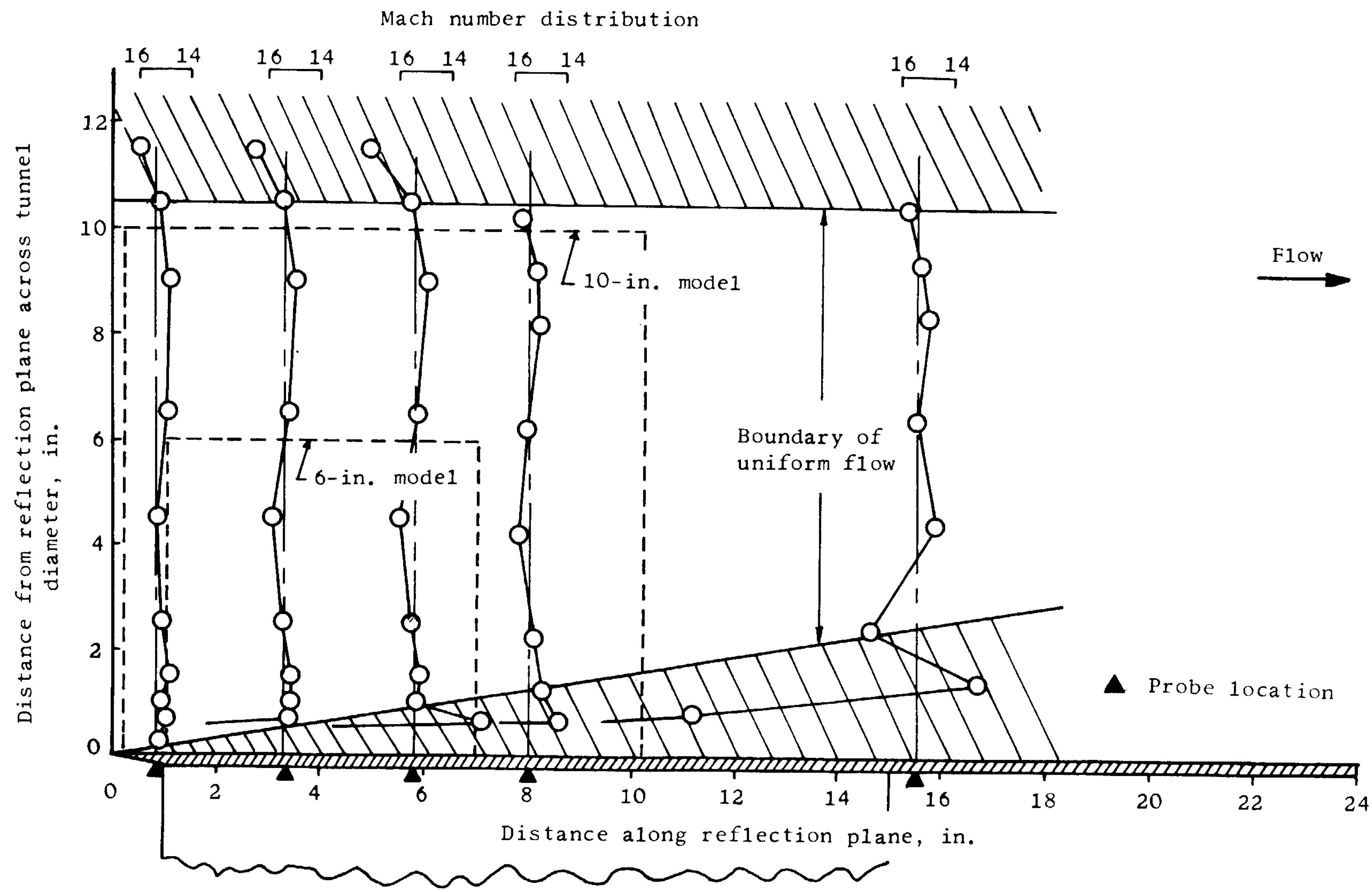

Figure 5.- Mach number survey in the plane of the model. Stagnation pressure, 750 lb/sq in.

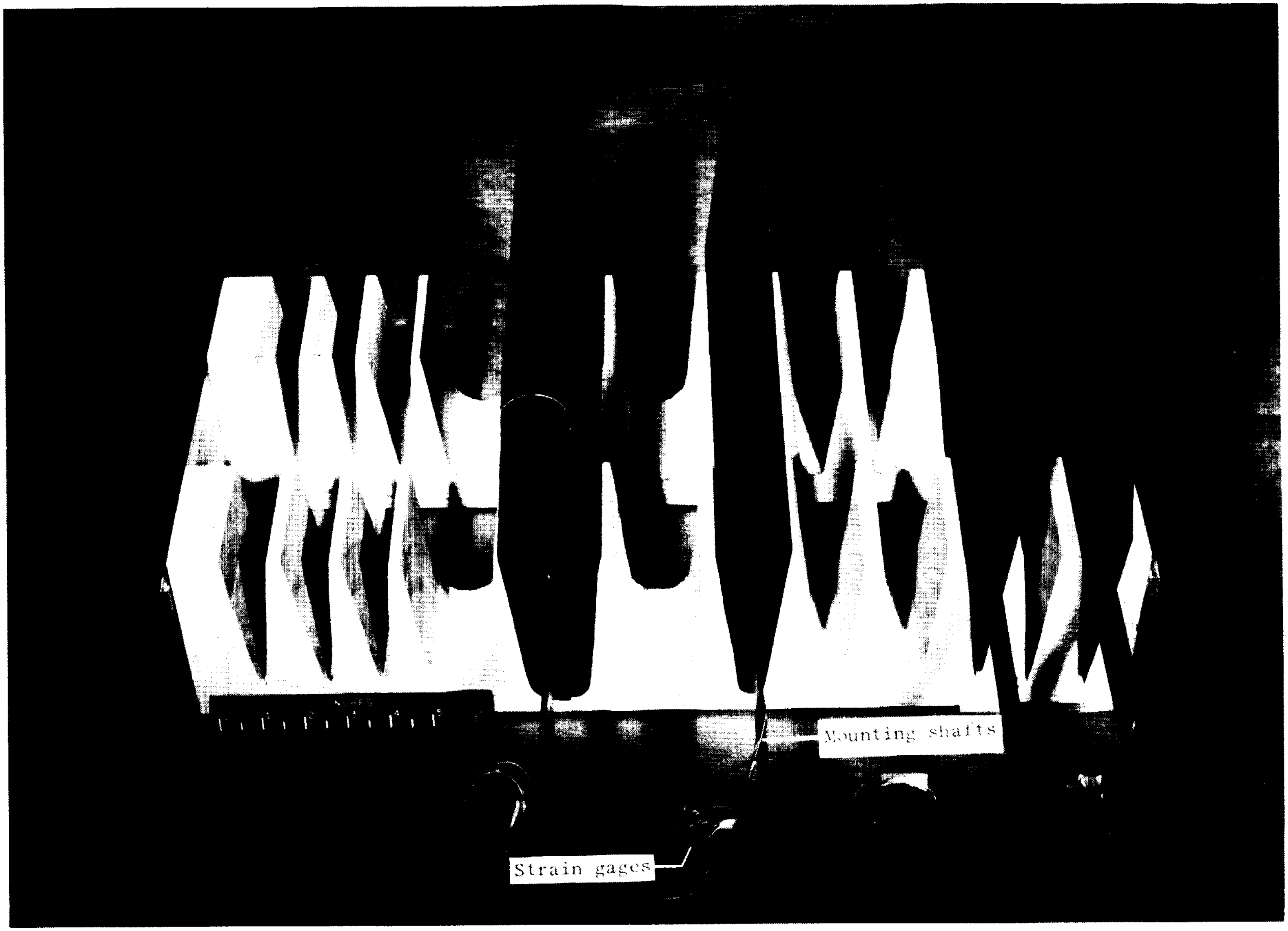

Figure 6.- Model profiles tested. L-61-1768.1

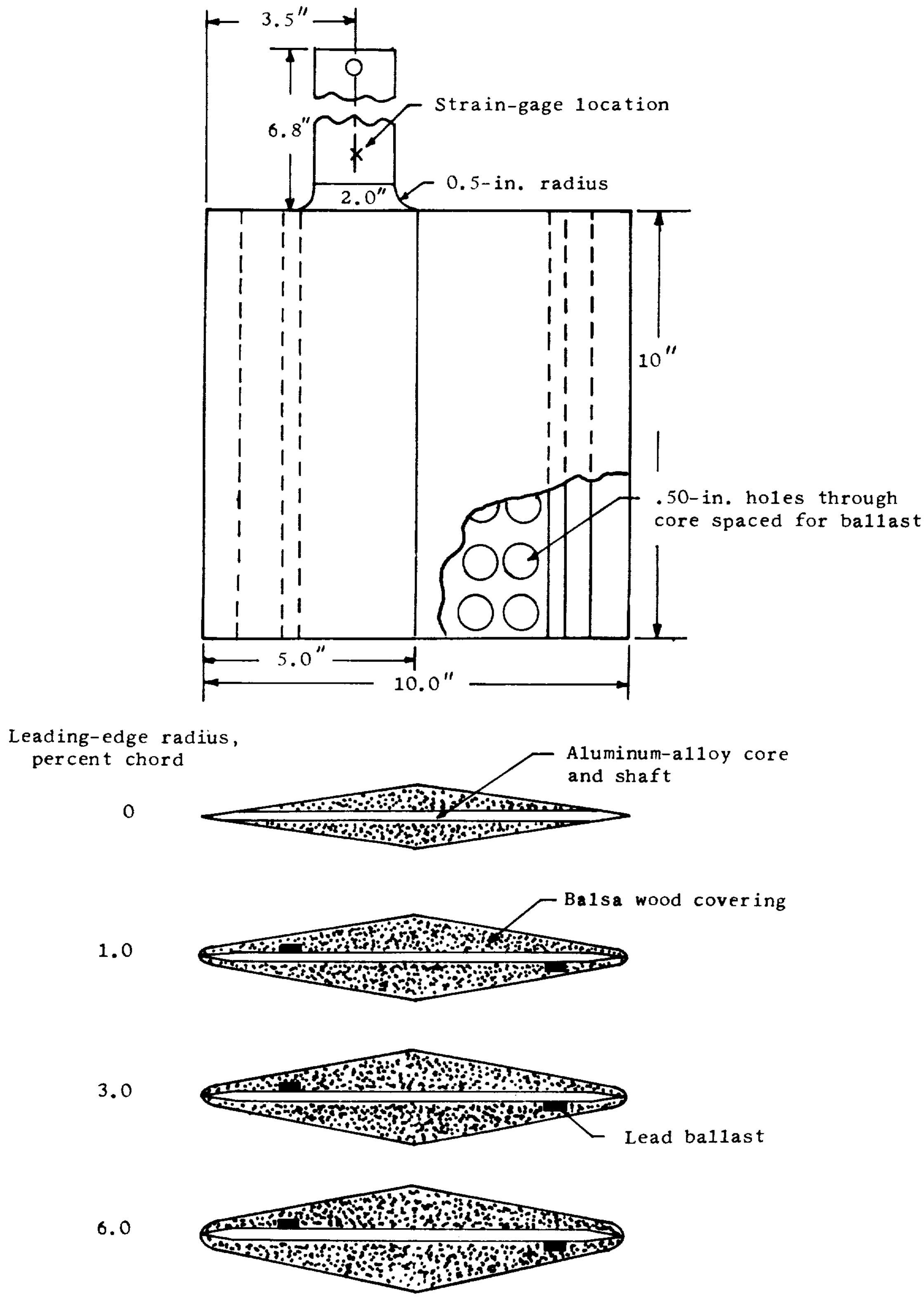

Figure 7.- Geometry and construction of 10-inch model series.

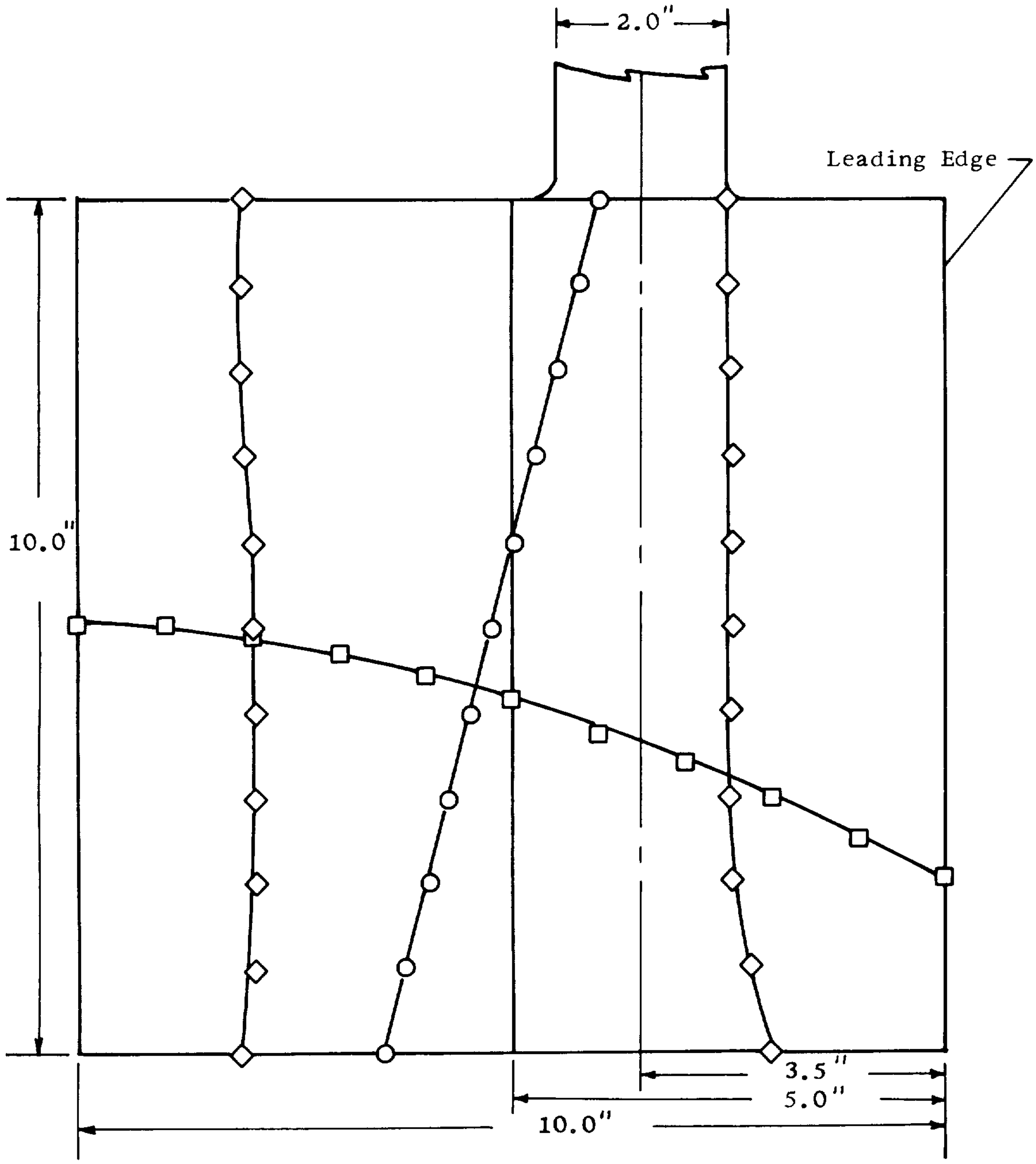

Frequency, cps	Mode
6.0	Flapping
○ 22.5	Pitching
□ 77.0	Second flapping
◇ 213.0	Second pitching

Figure 8.- Typical nodal patterns of models.

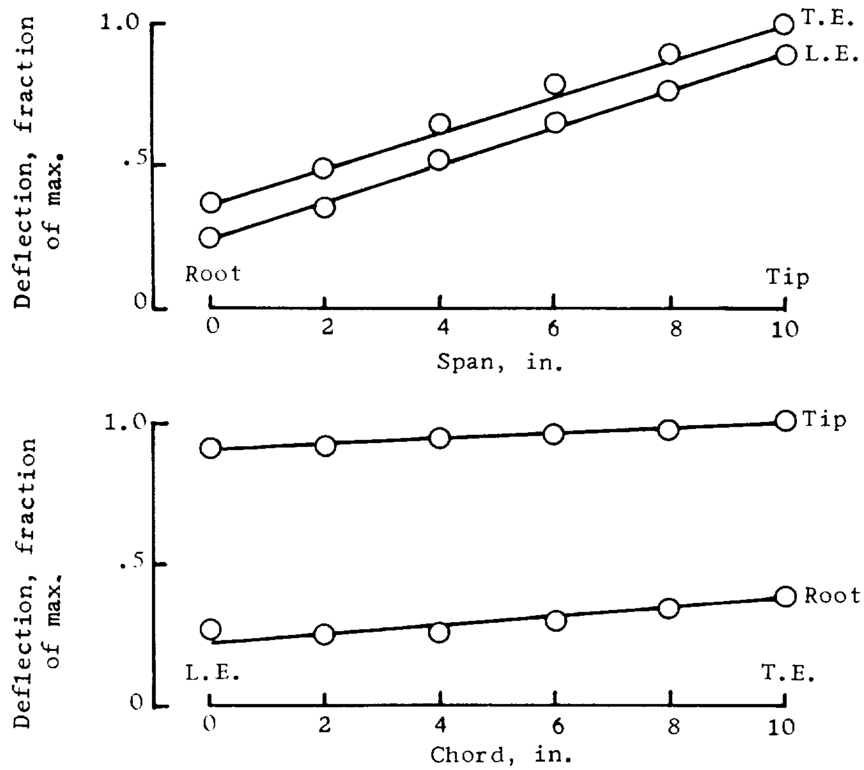

(a) Flapping mode.

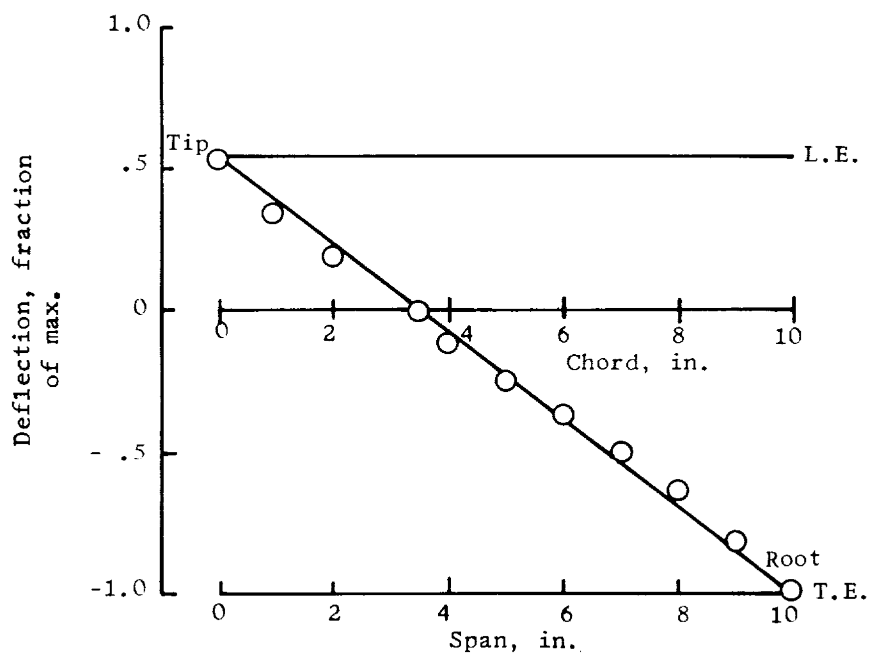

(b) Uncoupled pitching mode.

Figure 9.- Typical mode shape of flapping and uncoupled pitching modes.

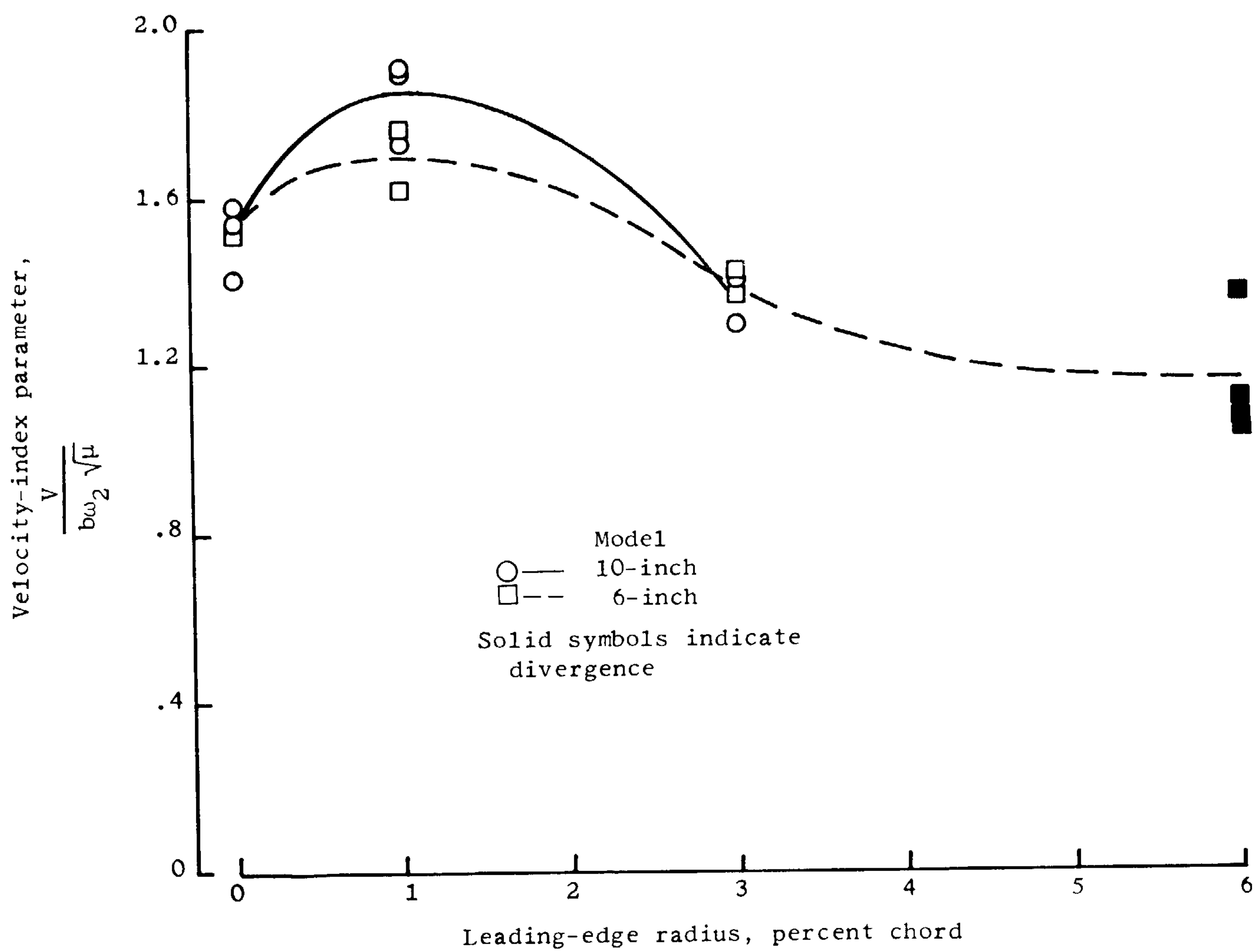

Figure 10.- Variation of velocity-index parameter as a function of leading-edge radius.

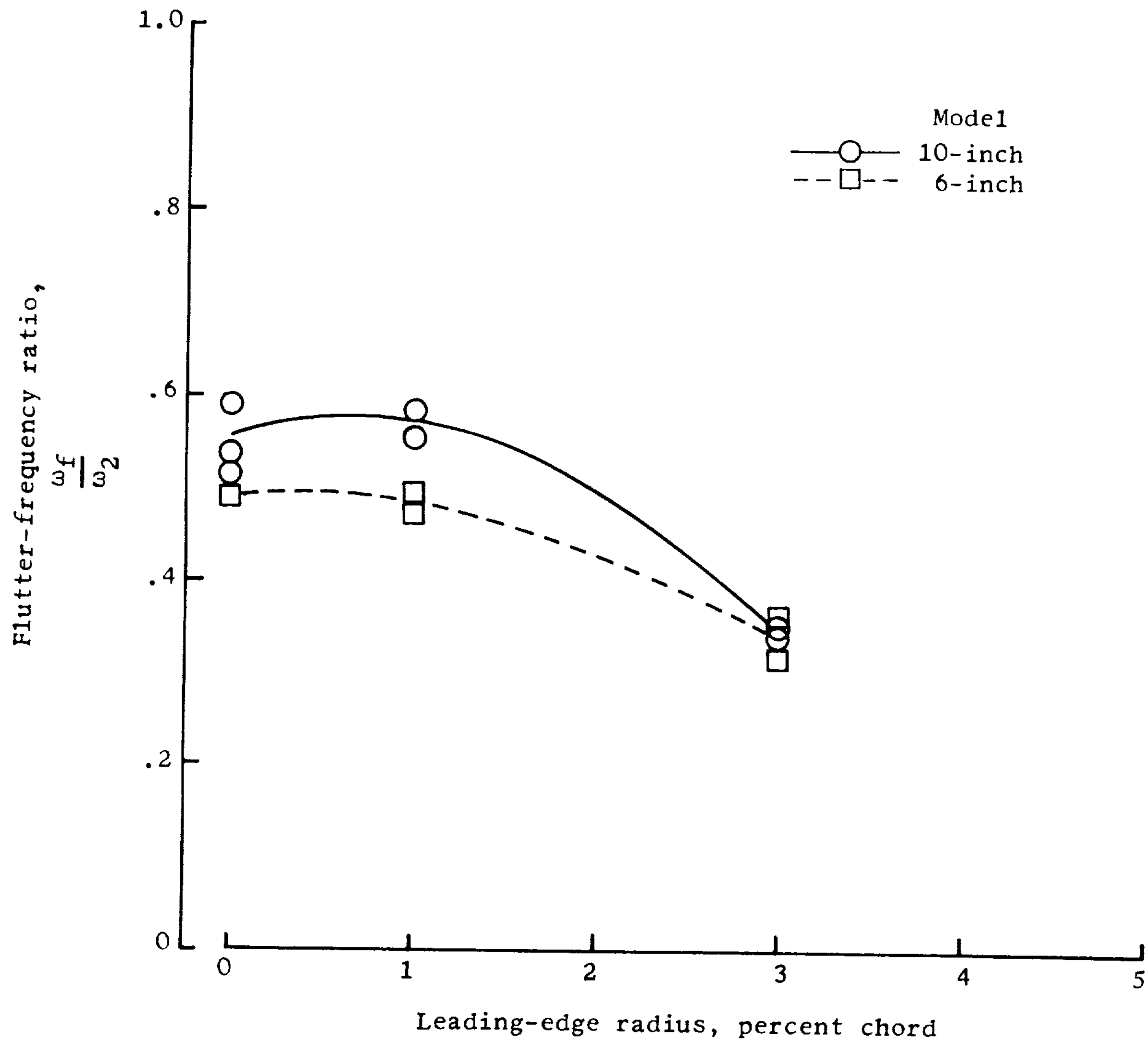

Figure 11.- Variation of flutter-frequency ratio with leading-edge radius.

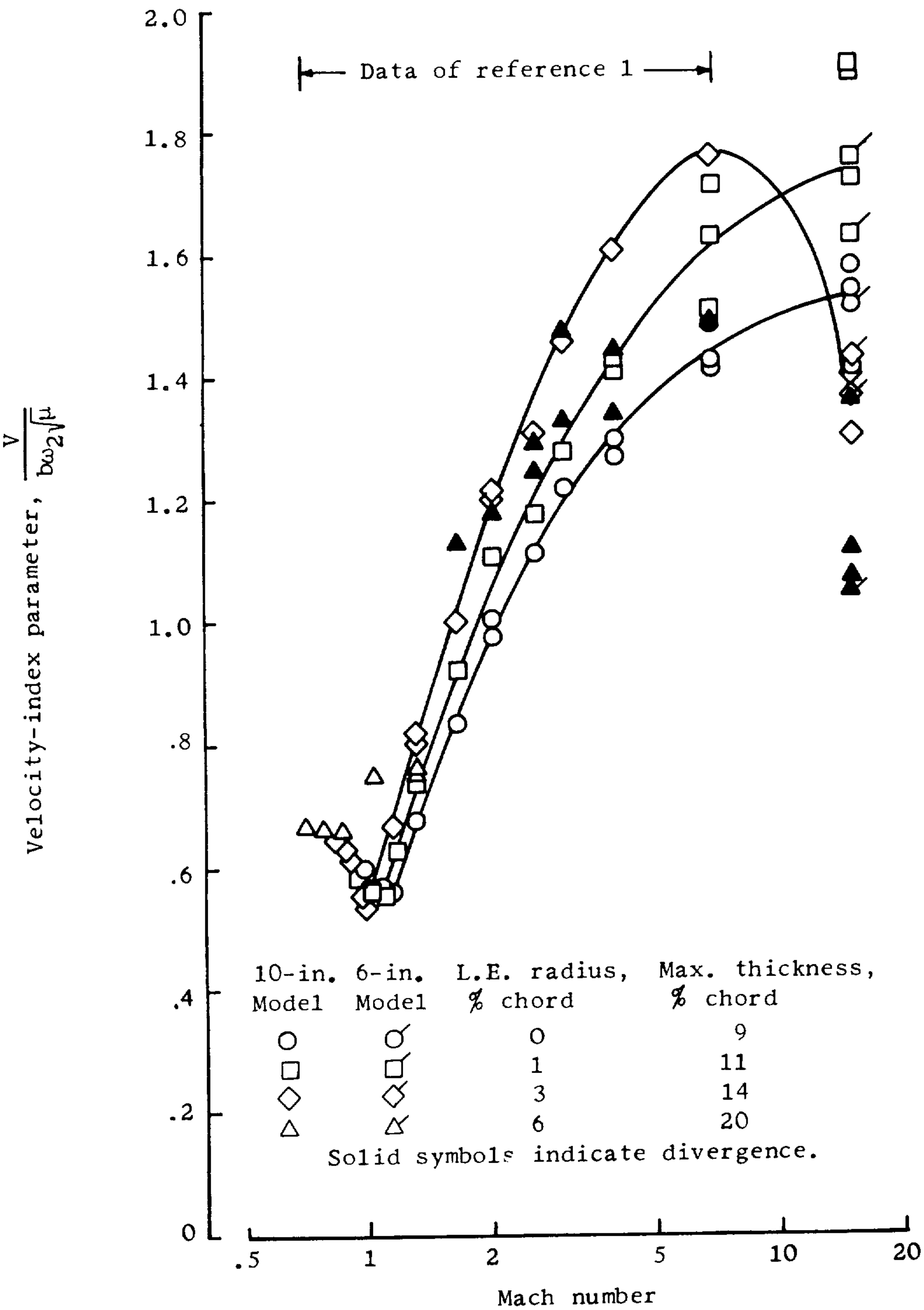

Figure 12.- Variation of velocity-index parameter with Mach number for double-wedge airfoils with blunt leading edges.

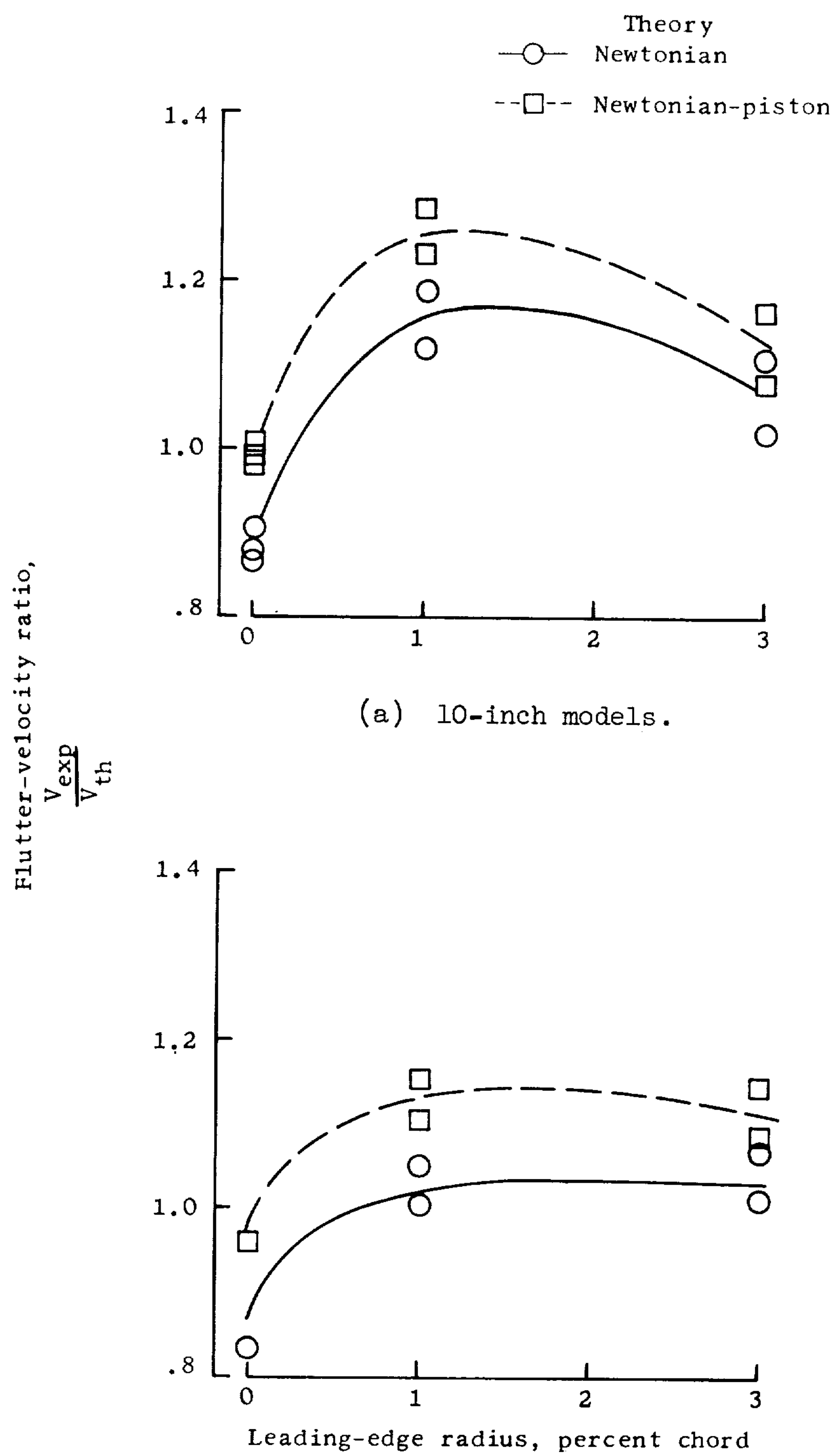

(a) 10-inch models.

(b) 6-inch models.

Figure 13.- Ratio of experimental to calculated flutter velocity as a function of leading-edge radius.

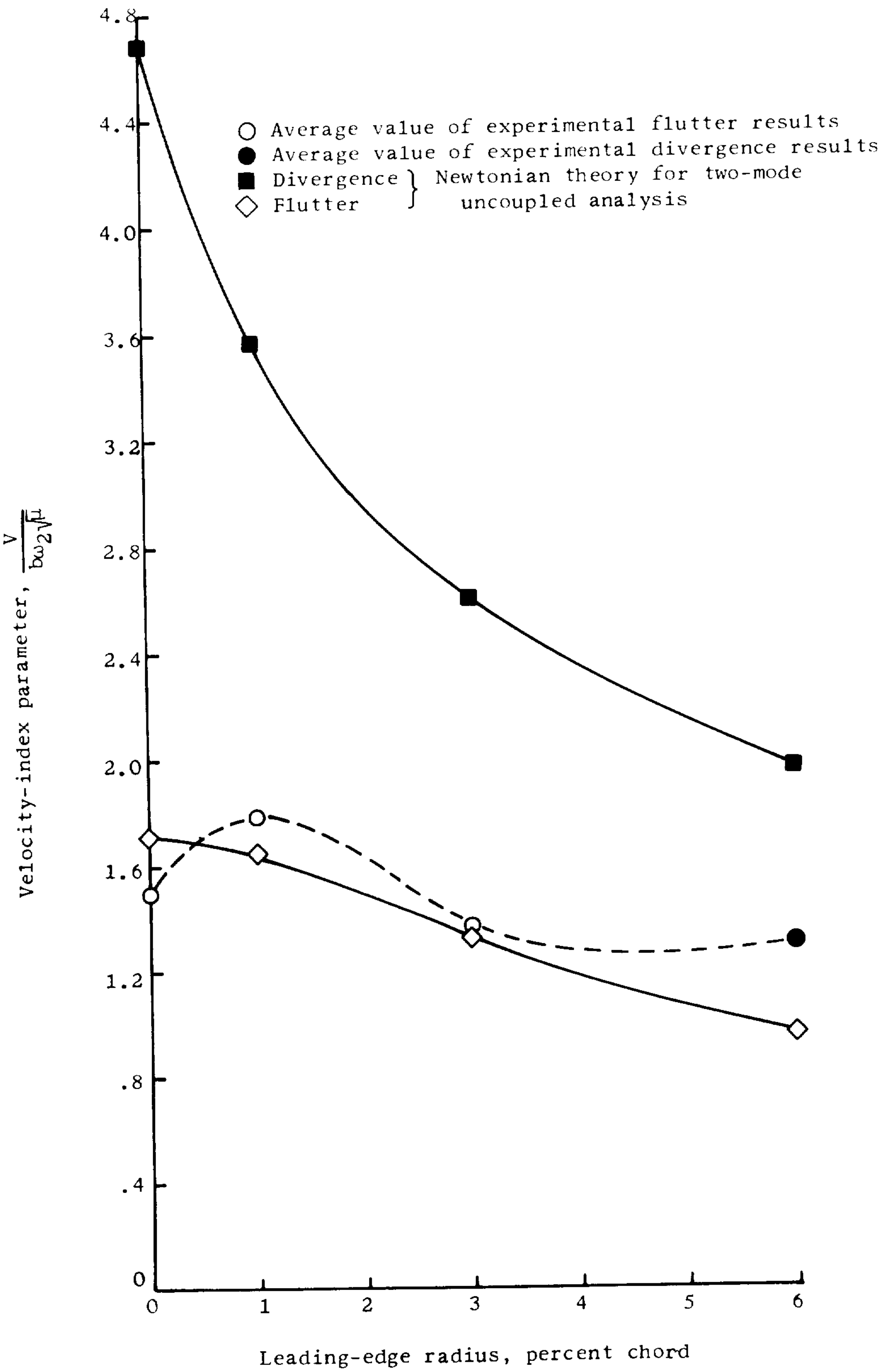

Figure 15.- Velocity-index trends with leading-edge bluntness.

NASA-Langley, 1962 L-2034

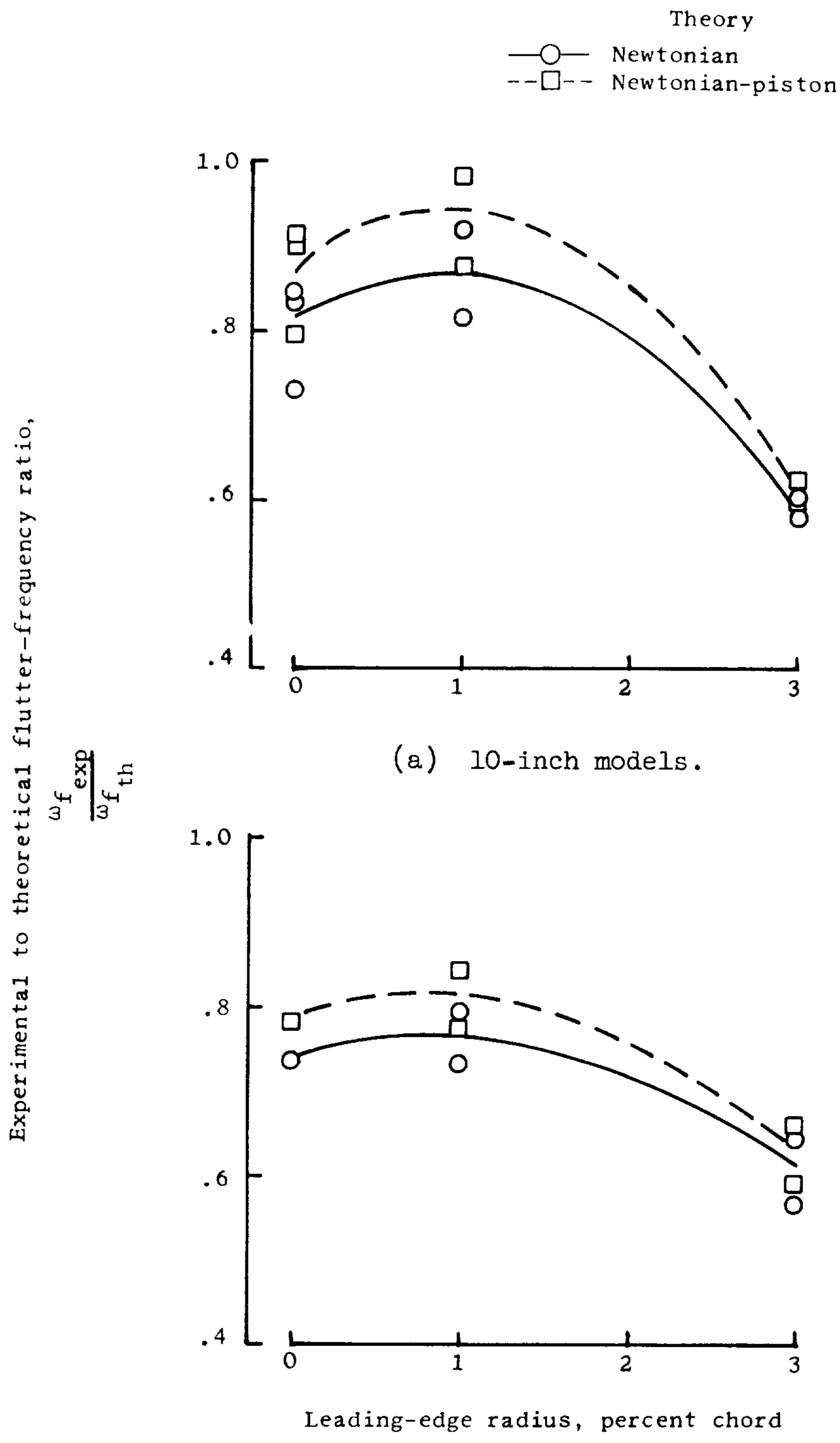

Figure 14.- Variation of experimental to theoretical flutter-frequency ratio as a function of leading-edge radii.